An algorithm for computed tomography image reconstruction from limited-view projections*

Wang Lin-Yuan(王林元)[a)], Li Lei(李 磊)[a)], Yan Bin(闫 镔)[a)†],
Jiang Cheng-Shun(江成顺)[a)], Wang Hao-Yu(王浩宇)[b)], and Bao Shang-Lian(包尚联)[b)]

[a)] *National Digital Switching System Engineering & Technological R&D Centre, Zhengzhou* 450002, *China*
[b)] *The Beijing City Key Lab of Medical Physics & Engineering, Peking University, Beijing* 100871, *China*

(Received 4 November 2009; revised manuscript received 13 December 2009)

With the development of the compressive sensing theory, the image reconstruction from the projections viewed in limited angles is one of the hot problems in the research of computed tomography technology. This paper develops an iterative algorithm for image reconstruction, which can fit most cases. This method gives an image reconstruction flow with the difference image vector, which is based on the concept that the difference image vector between the reconstructed and the reference image is sparse enough. Then the l_1-norm minimization method is used to reconstruct the difference vector to recover the image for flat subjects in limited angles. The algorithm has been tested with a thin planar phantom and a real object in limited-view projection data. Moreover, all the studies showed the satisfactory results in accuracy at a rather high reconstruction speed.

Keywords: limited-view problem, computed tomography image reconstruction algorithms, reconstruction-reference difference algorithm, adaptive steepest descent-projection onto convex sets algorithm

PACC: 8170J, 8760G, 0420J

1. Introduction

Image reconstruction algorithms implemented in existing computed tomography (CT) scanners require that the projection data should be available in proportional-space.[1,2] However, in practical applications, the projection data often are acquired only in a limited angle range. This situation is referred to as the limited-view problem (LVP). The LVP arises when the number of views is restricted by data collection time or by geometric constraints in the scan structure of the imaging system itself. In order to solve this problem, iterative methods are usually employed.

Algebraic reconstruction technique (ART) is one of the widely used iterative methods in a system of discrete linear equations for a weighted summing process of corresponding voxels. Much work has been done on developing iterative methods for CT image reconstruction using both linear and nonlinear system models.[2−7] Recently, a new iterative algorithm was developed based on constrained, total-variation (TV) minimization,[8−11] which was an optimized method from compressive sensing (CS) theory by Candes *et al.* using discrete Fourier transform.[8] A preliminary study of constrained, TV-minimization algorithms has been conducted to inversion of the x-ray transform from limited numbers and ranges of scanning views.[10−14]

The CS theory by Candes *et al.* turns out that the sparse image could be found by solving the convex optimization problem of minimizing the l_1-norm of the image.[8,9] Based on l_1-norm minimization, we have investigated image reconstruction employing projection matrix directly.[15] Non-convex optimisation formulations are investigated. Their conclusion is that based on the l_1-norm minimisation, TV method could potentially be improved in limited-view.[13,16] In fact, TV is a method derived from l_1-norm of the gradient-magnitude images (GMI).[11] In this paper, we develop a kind of l_1-norm minimisation iterative algorithm for LVP.

*Project supported by the National Basic Research Program of China (Grant No. 2006CB7057005), the National High Technology Research and Development Program of China (Grant No. 2009AA012200), and the National Natural Science Foundation of China (Grant No. 60672104).
†Corresponding author. E-mail: tom.yan@gmail.com
© 2010 Chinese Physical Society and IOP Publishing Ltd

2. Theory

The adaptive steepest descent (ASD)-projection onto convex sets (POCS) algorithm from the work[11] by Sidky *et al.* is described as a reference. Then, we develop a reconstruction-reference difference (RRD) algorithm with l_1-norm minimization for image reconstruction in circular cone-beam CT.

2.1. The ASD–POCS algorithm

The imaging model can be approximated by the following system of discrete linear equations:

$$g = M\boldsymbol{f}, \tag{1}$$

where the vector g has length $N_{\rm d}$, which is the number of measured projection rays; the vector $\boldsymbol{f}$ has length $N_{\rm im}$, which is the number of expansion elements used in representing the object function $f(\boldsymbol{r})$, the system matrix M is a ray-driven projection operator.

Having approximated image reconstruction for circular cone-beam CT to inversion of a finite linear system, we find that constrained TV minimization yields the discrete image $\boldsymbol{f}$ which minimizes its TV

$$\boldsymbol{f}^* = \arg\min \|\boldsymbol{f}\|_{\rm TV}\,. \tag{2}$$

Subject to the following inequality constraints: (A) data fidelity

$$|M\boldsymbol{f} - g_{\rm data}| \leq \varepsilon, \tag{3}$$

(B) non-negativity

$$\boldsymbol{f} \geq 0. \tag{4}$$

The ASD–POCS algorithm uses ASD algorithm for TV minimization and employs ART algorithm to keep data fidelity. Besides TV minimization, there are some alternative ways to get a sparse vector for reconstruction.

The l_1-norm of the image vector is taken into consideration, and an algorithm is developed.

2.2. The RRD algorithm

A specific algorithm based on l_1-norm minimization for image reconstruction is investigated. For an image to be reconstructed, the discrete image vector $\boldsymbol{f}$ is generally not sparse, so l_1-norm minimization could not be employed directly. To describe it conveniently, the image vector which is very close to reconstructed image is called the reference image vector (RIV) in this paper. The image vector to be reconstructed here is defined as a difference between reconstructed image vector and an RIV. In this definition, if the RIV is suitable, the difference image vector is sparse enough to employ l_1-norm minimization. In some applications, the RIV can be obtained by prior knowledge. Considering the universality of the algorithm, we find that a preliminary reconstruction result is more suitable to be an RIV.

The specific algorithm can be described as follows:

Step 1

Obtain an RIV using a single iteration of ART. Perform a single iteration of ART to obtain an objective vector $\boldsymbol{f}_{\rm r}$, which is close to the reconstructed image vector:

$$\begin{aligned}\text{ART}: \boldsymbol{f}_{\rm r} :=\ & \boldsymbol{f}_{\rm r} + \beta \boldsymbol{M}_{\rm i}' \cdot (\boldsymbol{M}_{\rm i} \cdot \boldsymbol{M}_{\rm i}')^{-1} \\ & \cdot (g_{\rm i} - \boldsymbol{M}_{\rm i}\boldsymbol{f}_{\rm r}).\end{aligned} \tag{5}$$

Step 2

Obtain the projection images of the sparse vector. Generate projection images with the RIV in each view first:

$$g_{\rm r} = M\boldsymbol{f}_{\rm r}. \tag{6}$$

Then obtain new projection images by taking generated images from collected images:

$$\Delta g = g - g_{\rm r}. \tag{7}$$

The new images could be considered as the projections from the sparse image vector defined above.

Step 3

Reconstruct the sparse image vector employing l_1-norm minimization:

$$\boldsymbol{f}_{\Delta}^* = \arg\min \|\boldsymbol{f}_{\Delta}\|_{l_1}\,. \tag{8}$$

Subject to the inequality constraints:

$$|M\boldsymbol{f}_{\Delta} - \Delta g| \leq \varepsilon. \tag{9}$$

The reconstructed image vector will be the sum of the sparse vector and the reference vector:

$$\boldsymbol{f} = \boldsymbol{f}_{\rm r} + \boldsymbol{f}_{\Delta}. \tag{10}$$

3. Results

3.1. Simulation

To demonstrate these two algorithms for image reconstruction from limited-view projections, we performed two simulation studies. The size of the phantom is 1024×10×1024, and the phantom makes up of

10 slices of two-dimensional Shepp–Logan phantom. The projections are modeled on the circular cone-beam CT configuration. For this situation in existing CT scanners, data from a limited range of angles is not available, and the LVP arises.

3.1.1. Reconstructions with the ASD-POCS algorithm

For this study, projection data were generated for the phantom at 36 views covering the full 360°. Because the phantom is flat, the data from 80° to 100° and from 260° to 280° were not used for the LVP. In fact, we reconstructed the object from 30 views. The first slice of the true image is shown in Fig. 1(a); the same slice of the reconstruction result is shown in Fig. 1(b). Furthermore, we display in Fig. 2 the profiles on the different straight lines through images shown in Fig. 1. Figures 2(a) and 2(b) display the profiles along the horizontal line specified by $y = 398$; figures 2(c) and 2(d) show the profiles along the vertical line specified by $x = 509$. The solid and dotted lines indicate the reconstructed and the corresponding true profiles, respectively.

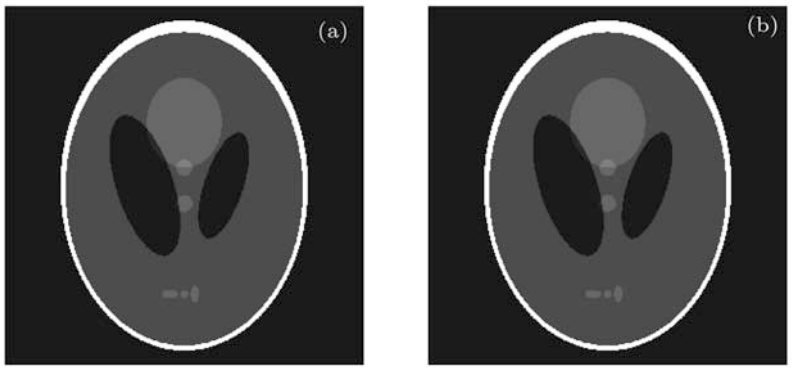


Fig. 1. Reconstruction result using ASD–POCS: (a) the first slice of the phantom; (b) the first slice of the reconstruction result by use of the ASD–POCS algorithm.

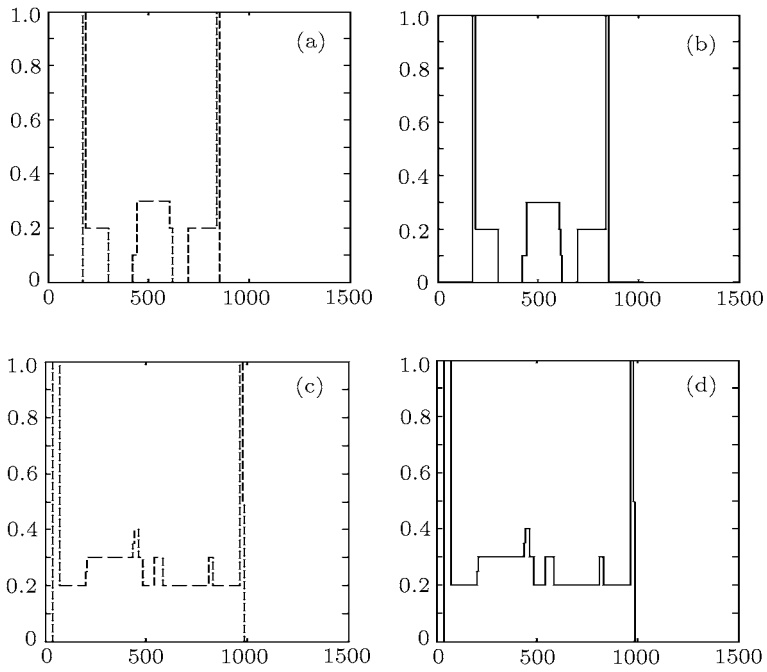


Fig. 2. Profiles of the reconstructed images in Fig. 1: (a) and (b) the profiles along x-axis at $y = 398$; (c) and (d) the profiles along y-axis at $x = 509$.

3.1.2. Reconstructions with the RRD algorithm

In this study, we also reconstructed the object from 30 of the 36 views as above. The first slice of the true image is shown in Fig. 3(a); the same slice of the reconstruction result is shown in Fig. 3(b). We display in Fig. 4 the profiles on the different straight lines through images shown in Fig. 3. Figures 4(a) and 4(b) display the profiles along the horizontal line specified by $y = 398$; figure 4(c) and 4(d) show the profiles along the vertical line specified by $x = 509$. The dotted curve represents the true value, and the solid curve represents the result obtained with our algorithm.

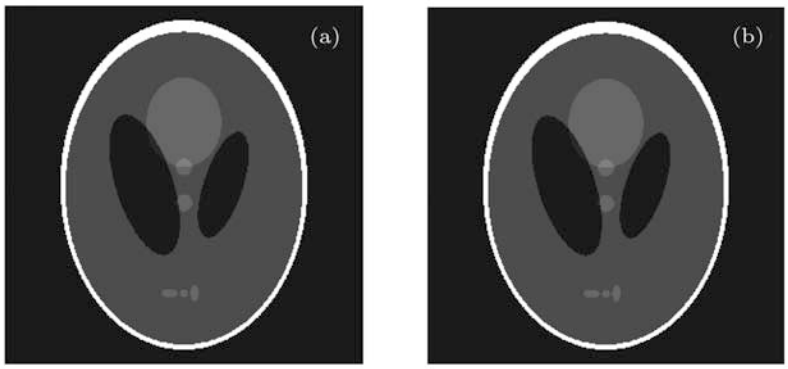


Fig. 3. Reconstruction result using RRD: (a) the first slice of the phantom; (b) the same slice of the reconstruction result obtained with our algorithm.

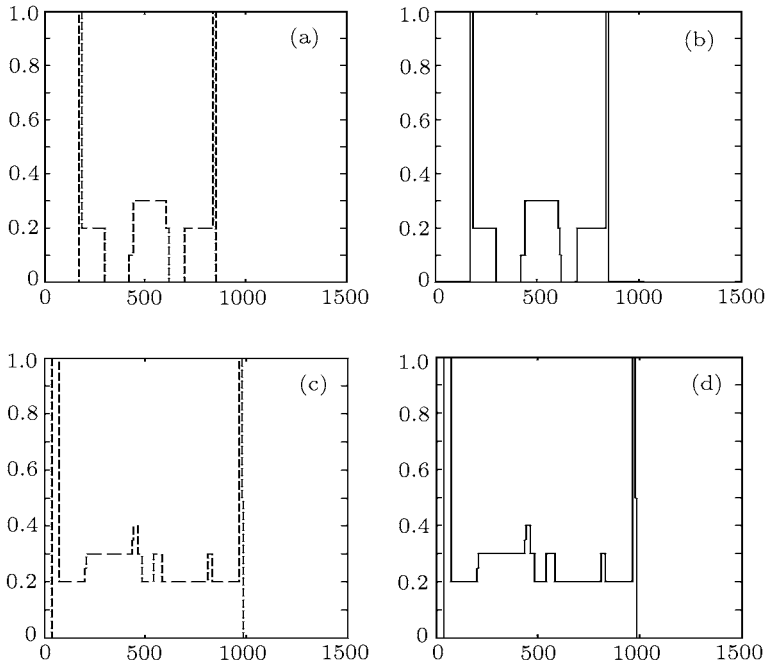


Fig. 4. Profiles of the reconstructed images in Fig. 3: (a) and (b) the profiles along x-axis at $y = 398$; (c) and (d) the profiles along y-axis at $x = 509$.

It appears that under the conditions of this idealized simulation, both of the two algorithms yield accurate reconstructions. Figures 1 and 3 show that the reconstructed results are very close to the true image. Moreover, the reconstructed profiles are almost identical to the true ones in Figs. 2 and 4.

3.2. Results from real data reconstruction

We further investigated the feasibility of using our method on real data. From the full 360 projections of original data, we extracted 72 projection images at angular views evenly distributed over the 2π circular

trajectory. To test the validity of the LVP, the data from 80° to 100° and from 260° to 280° were not used. We reconstructed a 256×256×512 image volume with an isotropic voxel size of 0.6 mm. Since there is no 'true image' to exactly represent the density distribution function, we used the Feldkamp–Davis–Kress (FDK) method to reconstruct the same three-dimensional volume using 72-view data for comparison.

We show in Fig. 5 the reconstructed image using the RRD algorithm. Also show the FDK reconstructed image on the 72-view data. Each image shown is displayed at a coronal ($y = 200$) plane. Same display window is used for both of the images in Fig. 5. It is clearly shown that the RRD algorithm successfully recovers almost all the details of the structures, and the image quality obtained by use of the RRD algorithm does not rapidly reduce as FDK as the number of projection views decreases.

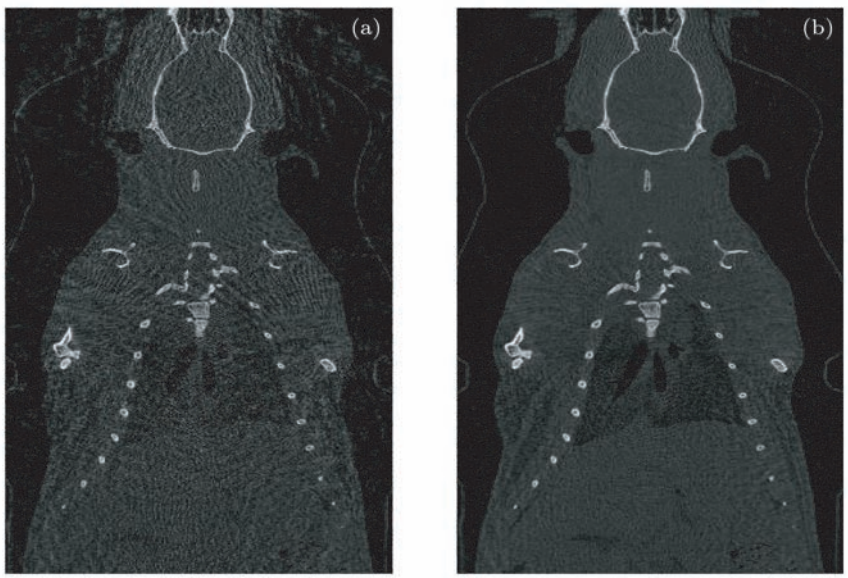


Fig. 5. Reconstructed images at a coronal plane ($y = 200$) using FDK and RRD: (a) the FDK reconstructed image was obtained from 72-view data; (b) the RRD image was reconstructed from 62 views.

4. Discussion

The results of the simulations show that both algorithms could be applied to the LVP. The RRD algorithm may yield accurate image reconstruction as well as the ASD–POCS algorithm even when the projection data are highly under-sampled. We have applied the RRD algorithm to real cone-beam data sets acquired at a number of views much smaller than what is used in current practice. Comparison with FDK suggests that the proposed algorithm can achieve good reconstruction with substantially reduced number of projections.

The main problem in the ASD–POCS algorithm is how to find a system to balance TV-gradient descent with POCS.[11] However, the same problem may not exist in the RRD algorithm. Moreover, the RRD algorithm only needs to use the ART once.

Besides GMI, there are some alternative transformations such as discrete wavelet transform and discrete cosine transform that could make the image sparse. Moreover, these two algorithms are of constrained TV minimization and l_1-norm minimization, but other convex objective functions also could be employed.

There is also the possibility of using more efficient operations or graphics processing unit acceleration.[17]

5. Conclusion

In this article, we have developed an RRD algorithm for image reconstruction which aims at solving the LVP. It has been demonstrated in computer simulation studies and real data studies that this algorithm is suitable for this problem and image reconstruction for flat subjects. Although the simulations presented here are based

on circular cone-beam CT, clearly the algorithm can be applied to other tomographic imaging modalities with linear system models.

In future work, we will apply the algorithm to real data sets more from x-ray based tomographic scanning systems. Also, we will make effort in reducing memory load and computation time.

References

[1] Andersen A H 1989 *IEEE Trans. Med. Imag.* **8** 50

[2] Lange K and Carson R 1984 *Comput. Assist. Tomogr.* **8** 306

[3] Sauer K and Bouman C 1993 *IEEE Trans. Signal Process* **41** 534

[4] Manglos S H, Gagne G M, Krol A, Thomas F D and Narayanaswamy R 1995 *Phys. Med. Biol.* **40** 1225

[5] Elbakri I A and Fessler J A 2003 *Phys. Med. Biol.* **48** 2453

[6] Kole J S 2005 *Phys. Med. Biol.* **50** 1533

[7] Zbijewski W, Defrise M, Viergever M A and Beekman F J 2007 *Phys. Med. Biol.* **52** 403

[8] Candes E, Romberg J and Tao T 2006 *IEEE Trans. Inf. Theory* **52** 489

[9] Candes E, Romberg J and Tao T 2006 *Commun. Pure Appl. Math.* **59** 1207

[10] Sidky E Y, Kao C M and Pan X C 2006 *X-ray Sci. Technol.* **14** 119

[11] Sidky E Y and Pan X C 2008 *Phys. Med. Biol.* **53** 4777

[12] Sidky E Y and Pan X C 2006 *IEEE Nucl. Sci. Conf. Rec.* **5** 2904

[13] Sidky E Y, Chartrand R and Pan X C 2007 *IEEE Nucl. Sci. Conf. Rec.* **5** 3526

[14] LaRoque S J, Sidky E Y and Pan X C 2008 *Opt. Soc. Am.* A **25** 1772

[15] Wang L Y, Jiang C S, Li L, Lu H H and Yan B 2008 *Proceedings of Great Wall* 2008 *International Congress on Medical Physics and The 14th National Annual Meeting of Medical Physics* p. 139

[16] Chartrand and Rick 2007 *IEEE Signal Process Lett.* **14** 707

[17] Xu F and Mueller K 2007 *Phys. Med. Biol.* **52** 3405